

A time-of-flight mass spectrometric study of laser fluence dependencies in SnO₂ ablation: implications for pulsed laser deposited tin oxide thin films

Haiyan Fan, Wei Ho, Scott A. Reid*

Department of Chemistry, Marquette University, P.O. Box 1881, Milwaukee, WI 53201-1881, USA

Received 6 May 2003; accepted 30 July 2003

Abstract

We report on a time-of-flight mass spectrometric study of laser fluence dependencies in the 532 nm ablation of SnO₂ targets. At all fluences investigated, SnO and Sn₂O₂ are the primary neutral gas-phase species. The relative yield of neutral tin-containing species increases exponentially up to a fluence of $\sim 1.9 \times 10^8 \text{ W cm}^{-2}$, and saturates at higher fluences. The yield of metal oxide clusters (primarily Sn₂O₂, Sn₄O₄) increases in the saturated region, while the yield of bare metal species (primarily Sn, Sn₂) decreases. In contrast, the peak kinetic energy of the primary neutral ablated species is insensitive to laser fluence in this range. These results support the hypothesis that the initial Sn:O stoichiometry of amorphous SnO_x films grown in vacuum using pulsed laser deposition (PLD) plays an important role in the formation of α -SnO during post-deposition annealing.

© 2003 Published by Elsevier B.V.

Keywords: Laser fluence; SnO₂; Pulsed laser deposition

1. Introduction

SnO₂ is a prototypical optically transparent n-type semiconductor that is widely used as a base material for the sensing of reducing gases [1–3]. Thin films have been synthesized by various means with pulsed laser deposition (PLD), a popular method [4–16]. In studies of SnO₂ films deposited on Si(001) substrates using 532 nm PLD from a compressed SnO₂ target [13,16], we found a strong correlation between deposition fluence and the phase transformations observed in post-deposition annealing. Specifically, the α -SnO phase appears only in films grown at laser fluences above $\sim 1.9 \times 10^8 \text{ W cm}^{-2}$, irrespective of film thickness [16]. To understand the origin of this phenomenon, we have extended our earlier work in mass spectrometric analysis of tin oxide ablation [17,18] to examine fluence dependencies in the composition and energetics of material ablated from an SnO₂ target at 532 nm, and these results are the focus of this report. We emphasize that these experiments exclusively probe the neutral ablation pathways.

2. Experimental methods

A detailed description of the experimental apparatus may be found in [17]. Briefly, SnO₂ targets were fabricated by cold pressing SnO₂ powder (Aldrich, purity >99.9%) at a typical pressure of 6000 psi, followed by annealing at $\sim 1450 \text{ K}$ for typically 60 h. The cylindrical targets were mounted on a computer controlled linear-rotary motion feedthrough that was inserted into the source region of a linear time-of-flight mass spectrometer (TOFMS). This region was evacuated by a water baffled 4 in. diffusion pump (Varian VHS-4), and the flight tube by a 250 l s⁻¹ turbomolecular pump (Varian). Typical source and flight tube pressures were 3×10^{-7} and 10^{-7} mbar, respectively.

The ablation laser beam, derived from a frequency doubled Nd:YAG laser system (Continuum NY-61), was focused to a spot size of $\sim 1 \text{ mm}$ diameter and struck the target along the surface normal. To ensure a constant laser spatial profile, the fluence was varied using a 532 nm $\lambda/2$ plate and thin film polarizer combination (CVI). Ablated species passed through a 3 mm aperture located $\sim 30 \text{ mm}$ from the target and into the interaction region of the TOFMS, and were subsequently ionized by 118.2 nm photons generated

* Corresponding author. Tel.: +1-414-288-7565; fax: +1-414-288-7066.
E-mail address: scott.reid@mu.edu (S.A. Reid).

61 by frequency tripling the 355 nm output of a second Nd:YAG
 62 laser system (Continuum Surelite II) in Xe [19]. Ions were
 63 extracted under a typical potential of 2 kV and traveled a distance
 64 of ~ 118 cm prior to striking a dual microchannel plate
 65 detector. The detector signal was amplified ($25\times$) using a
 66 fast preamplifier and recorded by a multichannel scaler with
 67 a typical bin width of 5 ns. The ablation laser was triggered
 68 at 5 Hz, one-half the repetition rate of the ionization laser,
 69 affording shot-by-shot background subtraction. The typical
 70 mass resolution ($m/\Delta m$) was >200 at $m/z = 120$ amu.

71 Two types of data were collected. First, mass spectra were
 72 obtained over 25,000 laser shots at different laser fluences,
 73 with the delay between ablation and ionization laser initially
 74 set at $30\ \mu\text{s}$ and stepped by $7\ \mu\text{s}$ every 1000 shots in
 75 order to (approximately) integrate over the arrival time
 76 distribution. From these spectra the total neutral yield and
 77 relative yields of specific Sn-containing species as a function
 78 of laser fluence were obtained. Second, neutral arrival time
 79 (velocity) distributions were obtained by measuring the
 80 integrated mass signals for a given species as a function of the
 81 ablation-ionization laser delay, with the mass spectra typically
 82 accumulated over 2000 shots. Details concerning the
 83 fitting procedure are found in [17].

84 3. Results

85 We first examined the total neutral signal at a fixed neutral
 86 arrival time for all Sn-containing compounds, shown in Fig.
 87 1 over a fluence range of $\sim 5 \times 10^7$ to $5 \times 10^8\ \text{W cm}^{-2}$. The
 88 signal increases exponentially up to a fluence of $\sim 1.9 \times$

89 $10^8\ \text{W cm}^{-2}$, and saturates at higher fluences. We correlate
 90 the saturation point with the onset of ablation, or formation
 91 of a laser-induced plasma, by analogy with results obtained
 92 for a Sn metal target [17], where the saturation fluence is
 93 roughly correlated with the onset of visible emission from
 94 electronically excited neutral and ionized Sn atoms, and is
 95 similar to the reported threshold for ablation at 248 nm [20].

96 Fig. 2 displays the fluence dependence of the fractional
 97 yields of neutral Sn-containing compounds over the same
 98 range. A consistent trend toward loss of Sn and Sn_2 is
 99 observed, with an increase in yield of Sn_2O_2 and Sn_4O_4
 100 at higher fluence. These trends are more apparent in Fig.
 101 3, which compares the summed data for Sn_x and Sn_xO_y
 102 species. The apparent saturation of Sn_2O_2 signal at higher
 103 fluences is artificial, since cracking of this compound to SnO
 104 is observed at higher fluences, as quantified below. We note
 105 in passing that no new species appear in the mass spectrum
 106 over this fluence range, and the day-to-day reproducibility
 107 of the data at a given fluence was within a few percent.

108 The laser fluence dependence of the velocity (arrival time)
 109 distributions for the dominant species, SnO and Sn_2O_2 ,
 110 was investigated. As shown in Fig. 4, with increasing fluence
 111 the SnO distribution increasingly deviates from a single
 112 time-transformed Maxwell–Boltzmann (MB) distribution,
 113 and the onset of this trend occurs close to the saturation
 114 point observed in Fig. 1. The distribution at $2.2 \times$
 115 $10^8\ \text{W cm}^{-2}$ is fit reasonably well by a single MB distribution,
 116 but a close examination reveals a small contribution
 117 from a slower component, and an improved fit is obtained
 118 to a two-component MB distribution, as shown in Fig. 5a. These trends become clearer in the data obtained

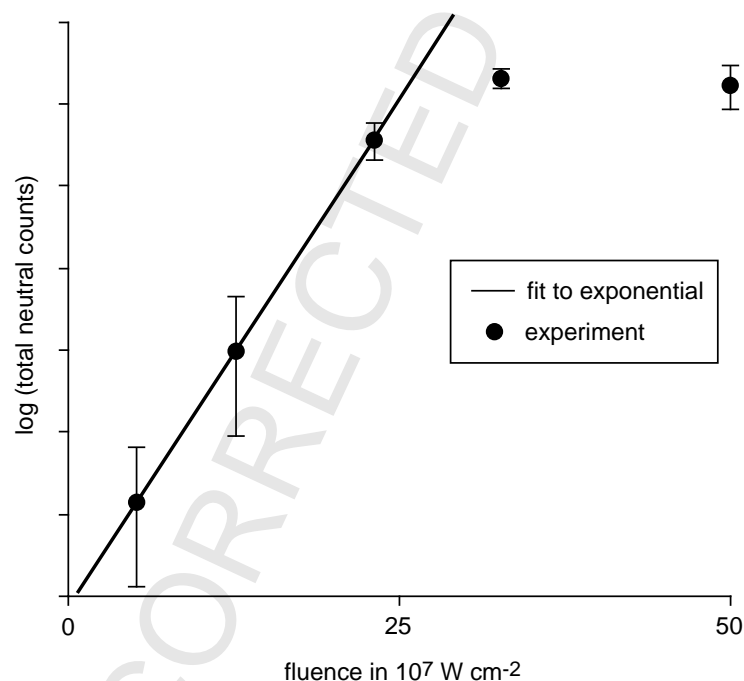


Fig. 1. Total neutral signal for all Sn-containing compounds as a function of laser fluence.

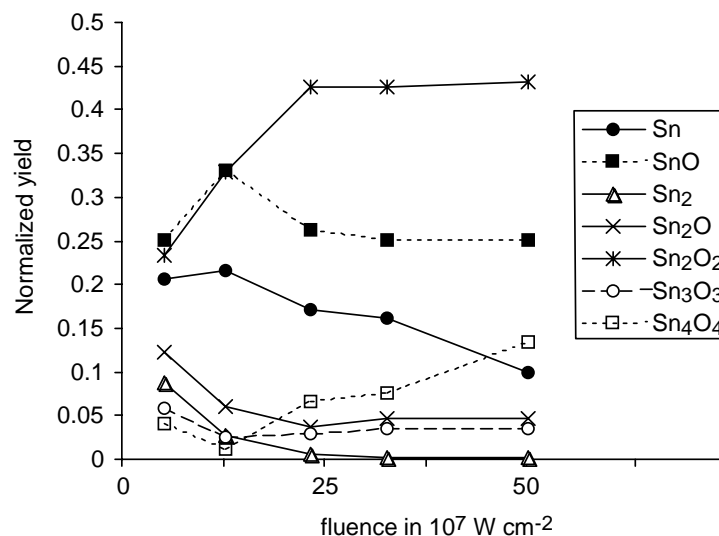


Fig. 2. Fluence dependence of the normalized yields of neutral Sn-containing species.

119 at $3.1 \times 10^8 \text{ W cm}^{-2}$, as shown in Figs. 4 and 5b. The fit
 120 parameters obtained for the slow component are essentially
 121 identical to those for Sn_2O_2 , and the Sn_2O_2 distributions at
 122 these fluences are well fit by a single MB distribution with
 123 t_{peak} set at the value obtained for the slow SnO component
 124 (Fig. 6). This result provides convincing evidence that the
 125 slow component arises from cracking of Sn_2O_2 in the ion-
 126 zation step, as discussed below.

127 Focusing on the primary component in the SnO distri-
 128 bution, we find a weak dependence of the peak velocity
 129 on fluence near and above the saturation point. For exam-
 130 ple, the distributions obtained at fluences of 2.2×10^8 and
 131 $3.1 \times 10^8 \text{ W cm}^{-2}$ give most probable speeds of 2.4×10^5
 132 and $2.5 \times 10^5 \text{ cm s}^{-1}$, respectively, with an uncertainty of
 133 $0.2 \times 10^5 \text{ cm s}^{-1}$. Similarly, for Sn_2O_2 the most probable
 134 speeds at these fluences are 1.41×10^5 and $1.36 \times 10^5 \text{ cm s}^{-1}$.
 135 In all cases the primary component is well fit by a single
 136 unshifted time-transformed MB distribution [17].

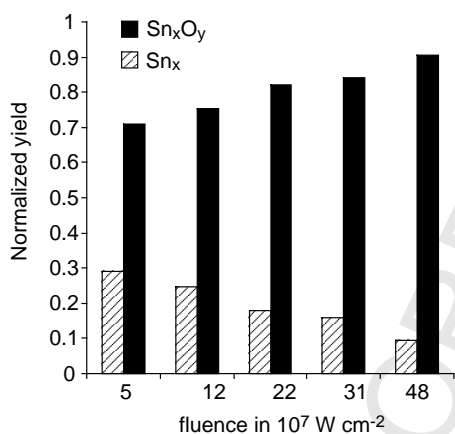


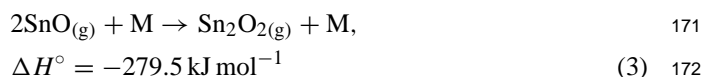
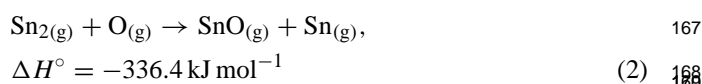
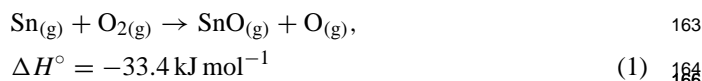
Fig. 3. Fluence dependence of the total neutral yield summed over all Sn_x and Sn_xO_y species.

4. Discussion

137

138 The major trends observed in the fluence dependence
 139 of the relative neutral yield (Fig. 2) are increases in both
 140 the yield of oxides, with concomitant loss of unoxidized
 141 species, and the yield of $(\text{SnO})_x$ clusters with increasing flu-
 142 ence. A similar trend has been observed in the ablation of
 143 a La–Ca–Mn–O target [21]. We emphasize that the relative
 144 photoionization efficiencies are unknown, and thus the rela-
 145 tive yields between species are only approximate. Moreover,
 146 the results shown in Fig. 2 were not corrected for fragmen-
 147 tation of Sn_2O_2 to SnO observed in the ionization step at the
 148 highest fluences, which would slightly increase the relative
 149 Sn_2O_2 :SnO yield.

150 A decrease in relative yield for a given neutral may re-
 151 flect its conversion into ions, or loss via photodissociation
 152 or secondary reactions in the gas-phase. The ionization
 153 potential of Sn (7.344 eV) is significantly smaller than that
 154 of SnO ($10.5 \pm 0.5 \text{ eV}$) [22], and the Sn_2 bond energy of
 155 2.1 eV is also smaller than that of the oxide clusters [22].
 156 Each of these mechanisms may therefore contribute. How-
 157 ever, the correlation observed in yield of unoxidized versus
 158 oxidized species (Fig. 3) and the increased yield of clusters
 159 at higher fluences suggest the importance of intraplume
 160 reactions [21], which may include (thermodynamic data
 161 from [23]):



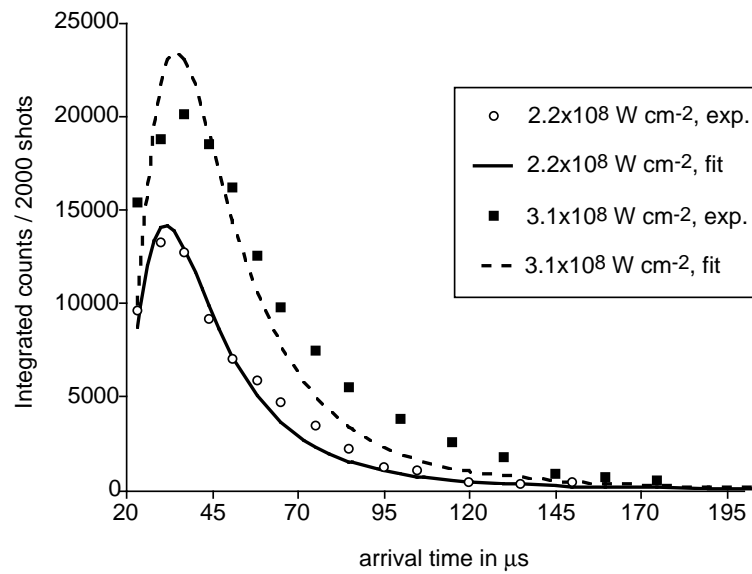


Fig. 4. SnO arrival time distributions (points) at two different laser fluences. The solid line in each plot is a fit to a single time-transformed Maxwell–Boltzmann distribution.

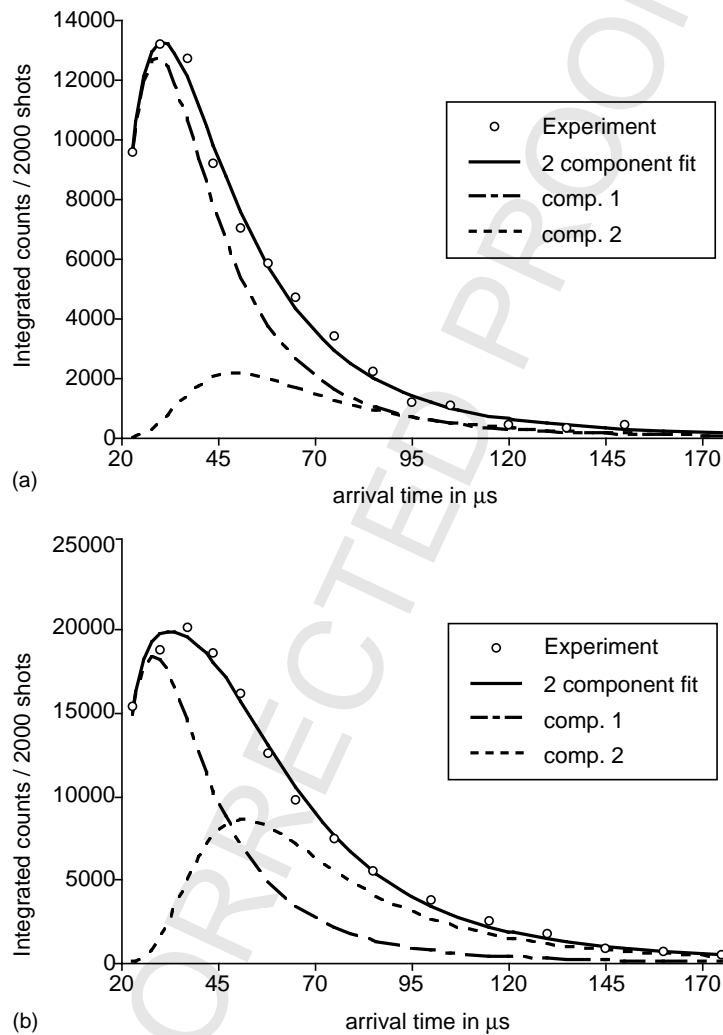


Fig. 5. SnO arrival time distributions (points) at fluences of (a) $2.2 \times 10^8 \text{ W cm}^{-2}$ and (b) $3.1 \times 10^8 \text{ W cm}^{-2}$. The distributions were fit to two-component time-transformed Maxwell–Boltzmann distributions, and each plot shows the two components and their sum.

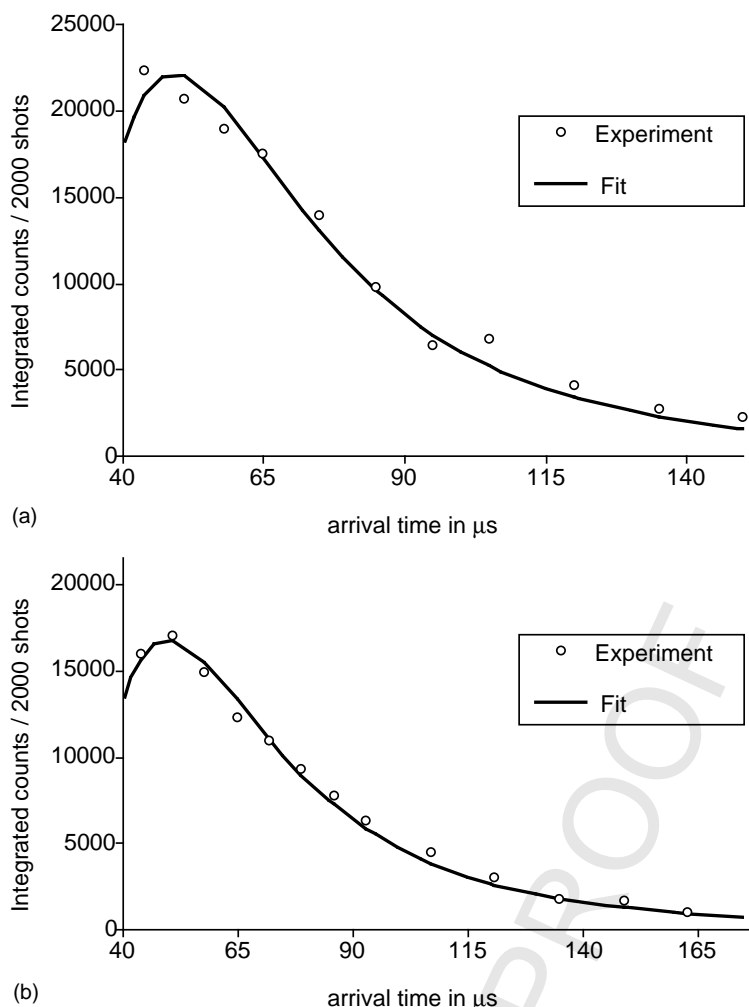
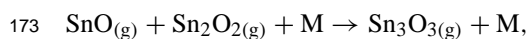
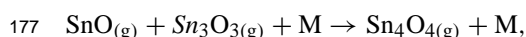


Fig. 6. Sn_2O_2 arrival time distributions (points) at fluences of (a) $2.2 \times 10^8 \text{ W cm}^{-2}$ and (b) $3.1 \times 10^8 \text{ W cm}^{-2}$. The solid line in each plot is a fit to a single Maxwell–Boltzmann distribution with t_{peak} set at the value obtained for the slow SnO component observed at the same fluence.



174 $\Delta H^\circ = -291.6 \text{ kJ mol}^{-1}$

(4)



178 $\Delta H^\circ = -297.5 \text{ kJ mol}^{-1}$

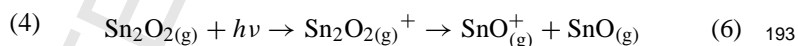
(5)

179 Detailed modeling of the intraplume chemistry is hampered
 180 by several factors, including our lack of knowledge of the
 181 kinetic parameters for reactions (1)–(5), and our inability
 182 to quantify the relative yields of O and O_2 [17]. How-
 183 ever, the kinetics of reaction (1) have been measured in the
 184 temperature range 380–1840 K, and the rate constant for this
 185 spin-allowed reaction is large, approaching $2 \times 10^{-10} \text{ cm}^3$
 186 $\text{molecule}^{-1} \text{ s}^{-1}$ at the highest temperatures [24,25].

187 As noted above, the SnO arrival time distributions become
 188 bimodal at fluences near the saturation point, and the corre-
 189 lation of the arrival time distribution of the slow component
 190 with that of Sn_2O_2 suggests that it arises from fragmentation
 191 of Sn_2O_2 in the ionization step, following photoionization,
 secondary ionization via electron impact, or interaction with

residual 355 nm radiation. The former process, i.e.:

192



194 is endoergic by 3.33 eV for 118 nm photons [22], although it
 195 is possible that highly internally excited species are formed
 196 at high fluences. As a check, we investigated the arrival time
 197 distribution of Sn_4O_4 at a fluence of $4.8 \times 10^8 \text{ W cm}^{-2}$, as
 198 the cracking ionization of Sn_4O_4 to Sn_2O_2^+ upon electron
 199 impact has been reported [26]. The Sn_4O_4 distribution is
 200 found to peak near 110 μs , significantly slower than the pri-
 201 mary Sn_2O_2 component. However, a small contribution from
 202 a slow component peaking near 110 μs can be seen in the
 203 Sn_2O_2 distribution obtained under the same conditions, as
 204 shown in Fig. 7, which suggests that fragmentation is occur-
 205 ring at higher fluences, caused either by electron impact or
 206 residual 355 nm radiation. When integrating over the arrival
 207 time distributions, the contribution of SnO signal resulting
 208 from Sn_2O_2 fragmentation was found to be 16 and 36%, re-
 209 spectively, at fluences of 2.2×10^8 and $3.1 \times 10^8 \text{ W cm}^{-2}$,
 210 and was negligible at smaller fluences.

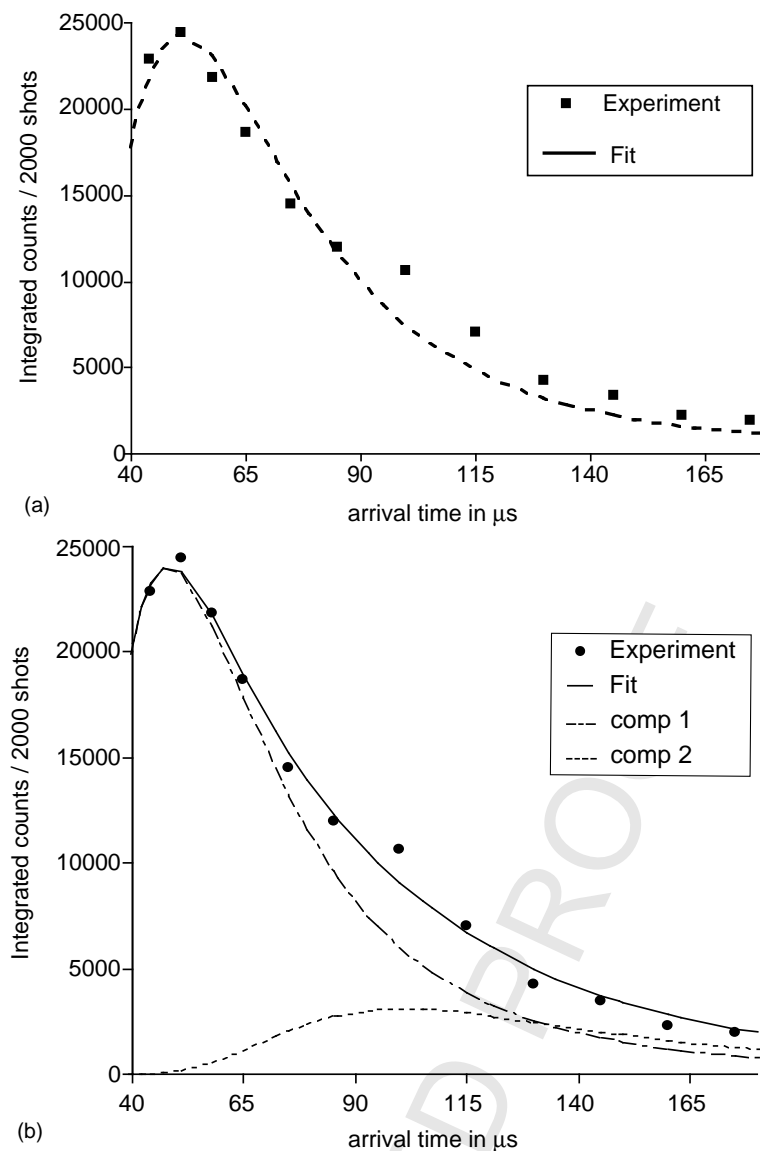


Fig. 7. Sn_2O_2 arrival time distribution at a fluence of $4.8 \times 10^8 \text{ W cm}^{-2}$ (points), fit to: (a) a single Maxwell–Boltzmann distribution, (b) a two-component MB distribution. The slow component has t_{peak} similar to that observed for Sn_4O_4 at the same fluence.

211 The primary arrival time distributions for SnO and Sn_2O_2 212
 213 are well fit by unshifted time-transformed MB distributions. 214
 215 This cannot be taken as evidence for a thermal mechanism, 216
 217 as previously discussed [17]. The importance of photochem- 218
 219 ical processes is evidenced in the peak kinetic energies, 220
 221 which are in all cases near the ablation photon energy and 222
 223 exhibit a weak dependence on laser fluence. 224

225 We now turn to trends observed in PLD generated SnO_x 226
 227 films [13,16]. We find that, for films grown in vacuum using 228
 229 532 nm PLD and subjected to post-deposition annealing in 230
 231 air, the formation of α - SnO is observed only for films grown 232
 233 at fluences above $\sim 1.9 \times 10^8 \text{ W cm}^{-2}$ [16]. The results pre- 234
 235 sented here show that the primary effect of increasing flu- 236
 237 ence is an increase in Sn:O stoichiometry of neutral species 238
 239 in the plume. In contrast, the peak kinetic energies of the 240
 241 primary neutral species are insensitive to laser fluence in this 242

227 range. These results support our initial hypothesis that the 228
 229 Sn:O stoichiometry of the amorphous film may govern the 230
 231 formation of α - SnO during post-deposition annealing [16]. 232
 233 Additional support is provided in the work of Muranaka et al. 234
 235 [27], who observed the formation of α - SnO from initially 236
 237 amorphous SnO_x ($x = 1.3$ – 1.5) films annealed in a nitrogen 238
 239 atmosphere. However, when the films were annealed in 240
 241 air, complete oxidation occurred prior to crystallization, and 242
 243 only r- SnO_2 (cassiterite) was observed. 244

5. Conclusions 236

237 We have reported a time-of-flight mass spectrometric 238
 239 study of fluence dependencies in the 532 nm ablation of 240
 241 SnO_2 targets. At all fluences in the range investigated, 242

240 SnO and Sn₂O₂ are the primary neutral gas-phase species.
 241 The relative yield of neutral Sn-containing species was
 242 found to increase exponentially for pulse energies below
 243 $\sim 1.9 \times 10^8 \text{ W cm}^{-2}$, and saturates at higher fluences. The
 244 yield of clusters such as Sn₂O₂ and Sn₄O₄ increases in the
 245 saturated region, while the yield of unoxidized species such
 246 as Sn and Sn₂ decreases, showing that the Sn:O stoichiometry
 247 of neutral species in the plume increases at higher laser
 248 fluences. In contrast, the peak kinetic energy of the primary
 249 neutral ablated species is insensitive to laser fluence in the
 250 range investigated. These results support our hypothesis that
 251 the initial Sn:O stoichiometry of amorphous SnO_x films
 252 grown using PLD plays an important role in the formation
 253 of α -SnO during post-deposition annealing.

254 References

- 255 [1] M.J. Madou, S.R. Morrison, *Chemical Sensing with Solid State*
 256 *Devices*, Academic Press, Boston, 1989.
- 257 [2] H. Iida, N. Shiba, T. Mishuku, H. Karasawa, A. Ito, M. Yamanaka,
 258 Y. Haiyashi, *IEEE Electron Device Lett.* EDL-4 (1983) 157.
- 259 [3] K. Takahata, in: T. Seiyama (Ed.), *Chemical Sensor Technology*,
 260 Elsevier, Amsterdam, 1988.
- 261 [4] A.N. Shatokhin, F.N. Putilin, O.V. Safonova, M.N. Rummyantseva,
 262 A.M. Gas'kov, *Inorg. Mater.* 38 (2002) 374.
- 263 [5] J.E. Dominguez, X.Q. Pan, L. Fu, P.A. Van Rompay, Z. Zhang, J.A.
 264 Nees, P.P. Pronko, *J. Appl. Phys.* 91 (2002) 1060.
- [6] W.S. Hu, Z.G. Lui, Z.C. Wu, D. Feng, *Mater. Lett.* 28 (1996) 369.
- [7] R.D. Vispute, V.P. Godbole, S.M. Chaudhari, S.M. Kanetkar, S.B. Ogale, *J. Mater. Res.* 3 (1988) 1180. 265
- [8] V.P. Godbole, R.D. Vispute, S.M. Chaudhari, S.M. Kanetkar, S.B. Ogale, *J. Mater. Res.* 5 (1990) 372. 266
- [9] R. Lal, R. Grover, R.D. Vispute, R. Viswanathan, V.P. Godbole, S.B. Ogale, *Thin Solid Films* 206 (1991) 88. 267
- [10] C.M. Dai, C.S. Su, D.S. Chuu, *Appl. Phys. Lett.* 57 (1990) 1879. 268
- [11] N.V. Morosova, A.M. Gas'kov, T.A. Kuznetsova, F.N. Putilin, M.N. Rummyantseva, V.I. Shatnov, *Inorg. Mater.* 32 (1996) 292. 269
- [12] W.S. Hu, Z.G. Liu, J.G. Zheng, X.B. Hu, X.L. Guo, W. Gopel, *J. Mater. Sci. Mater. Electron.* 8 (1997) 155. 270
- [13] F.J. Lamelas, S.A. Reid, *Phys. Rev. B* 60 (1999) 9347. 271
- [14] J.E. Dominguez, L. Fu, X.Q. Pan, *Appl. Phys. Lett.* 79 (2001) 614. 272
- [15] X.Q. Pan, L. Fu, J.E. Dominguez, *J. Appl. Phys.* 89 (2001) 6056. 273
- [16] H. Fan, S.A. Reid, *Chem. Mater.* 15 (2003) 564. 274
- [17] S.A. Reid, *Chem. Phys. Lett.* 301 (1999) 517. 275
- [18] S.A. Reid, W. Ho, F.J. Lamelas, *J. Phys. Chem. B* 104 (2000) 5324. 276
- [19] R. Mahon, T.J. McIlrath, V.P. Myerscough, D.W. Koopman, *IEEE J. Quant. Electron.* EQ-15 (1979) 444. 277
- [20] R. Timm, P.R. Willmott, J.R. Huber, *J. Appl. Phys.* 80 (1996) 1794. 278
- [21] H.J. Dang, Z.H. Han, Z.G. Dai, Q.Z. Qin, *Int. J. Mass Spectrom.* 178 (1998) 205. 279
- [22] A.A. Radzig, B.M. Smirnov, *Reference Data on Atoms, Molecules, and Ions*, Springer-Verlag, Berlin, 1985. 280
- [23] R.H. Lamoreaux, D.L. Hildenbrand, L. Brewer, *J. Phys. Chem. Ref. Data* 16 (1987) 419. 281
- [24] A. Fontijn, P.N. Bajaj, *J. Phys. Chem.* 100 (1996) 7085. 282
- [25] K. Takahashi, A. Giesen, P. Roth, *Chem. Phys. Phys. Chem.* 3 (2001) 4296. 283
- [26] E. Zimmerman, S. Königs, D. Neuschütz, *Z. Phys. Chem.* 193 (1996) 195. 284
- [27] S. Muranaka, B. Yoshichika, T. Takada, *Nippon Kagaku Kaishi* 11 (1987) 1886. 285
- 286
- 287
- 288
- 289
- 290
- 291
- 292
- 293
- 294
- 295
- 296
- 297